

A constrained von Mises distribution to describe fiber organization in thin soft tissues

Cecile L. M. Gouget · Michael J. Girard ·
C. Ross Ethier

Received: 24 December 2010 / Accepted: 20 June 2011 / Published online: 8 July 2011
© Springer-Verlag 2011

Abstract The semi-circular von Mises distribution is widely used to describe the unimodal planar organization of fibers in thin soft tissues. However, it cannot accurately describe the isotropic subpopulation of fibers present in such tissues, and therefore an improved mathematical description is needed. We present a modified distribution, formed as a weighted mixture of the semi-circular uniform distribution and the semi-circular von Mises distribution. It is described by three parameters: β , which weights the contribution from each mixture component; k , the fiber concentration factor; and θ_p , the preferred fiber orientation. This distribution was used to fit data obtained by small-angle light scattering experiments from various thin soft tissues. Initial use showed that satisfactory fits of fiber distributions could be obtained (error generally $< 1\%$), but at the cost of non-physically meaningful values of k and β . To address this issue, an empirical constraint between the parameters k and β was introduced, resulting in a constrained 2-parameter fiber distribution. Compared to the 3-parameter distribution, the constrained 2-parameter distribution fits experimental data well (error generally $< 2\%$) and had the advantage of producing physically meaningful parameter values. In addition, the constrained 2-parameter approach was more robust to experimental noise. The constrained 2-parameter fiber distribution can replace the semi-circular von Mises distribution to describe unimodal planar organization of fibers in thin soft tissues. Inclusion of such a function in constitutive models for

finite element simulations should provide better quantitative estimates of soft tissue biomechanics under normal and pathological conditions.

Keywords Collagen fiber organization · Semi-circular Von Mises distribution · Finite element implementation

1 Introduction

Collagen fibers have a major impact on the biomechanical properties of most soft tissues (Fung 1993), and computational models of such tissues should take into account the characteristics of the fibers and of their distribution. Indeed, tissue mechanical behavior depends strongly on the direction along which the fibers are aligned and on their degree of alignment (anisotropy). Here, we refer to “anisotropy” in the microstructural sense, i.e. to the degree of fiber alignment, recognizing that microstructural anisotropy implies mechanical anisotropy. In considering anisotropy, it is convenient to think of two limiting cases: a material in which all fibers are perfectly aligned in the plane of interest (transverse isotropy) and one in which the angular distribution of fibers is uniform in the plane of interest (planar isotropy). We give a quantitative measure of this behavior below.

Experimental techniques such as small-angle light/X-ray scattering (SALS/SAXS) (Chien and Chang 1972; McCally and Farrell 1982; Ferdman and Yannas 1993; Sacks et al. 1997; Bowes et al. 1999; Aghamohammadzadeh et al. 2004; Hayes et al. 2007; Abahussin et al. 2009; Joyce et al. 2009; Meek and Boote 2009), diffusion tensor imaging (Pierce et al. 2010) or 3D histology (Roberts et al. 2008) allow direct measurement of fiber distribution characteristics in tissues. However, these characteristics can depend strongly on position, so that it is necessary to make measurements at many dif-

C. L. M. Gouget · M. J. Girard · C. R. Ethier (✉)
Bioengineering, Imperial College London,
South Kensington Campus, London SW7 2AZ, UK
e-mail: r.ethier@imperial.ac.uk

C. L. M. Gouget
Département de Mécanique, Ecole Polytechnique,
Palaiseau, France

ferent locations. Hence, experiments typically lead to a large set of numerical data which must be incorporated into any modeling study of tissue biomechanics.

It is possible to directly use these data in finite element codes. However, it may be preferred to smooth these data and/or analyze the fiber characteristics directly, which is greatly facilitated by the use of a suitable mathematical function to fit the experimental data. The goal of this article was to discuss how this mathematical function can be chosen and optimized. We restrict attention to thin tissue samples, where the fibers lie predominantly within a (tangent) plane, so that the problem is two dimensional.

2 Methods

In principle, the approach we describe below can be used with a variety of experimental data. For this study, it was convenient to consider SALS data, a typical example of which is shown in Fig. 1. From such data, one obtains quantitative information on the fiber distribution at each experimental point: the angle $\theta_{p,\text{exp}}$ at the maximum of the distribution, referred to as the preferred fiber orientation (i.e. the modal angle); and the semi-circular variance, var_{exp} , a measure of the dispersion of the fibers around this angle. The quantity var_{exp} varies between 0 (transverse isotropy) and 1 (planar isotropy) and is defined as:

$$\text{var}_{\text{exp}} = 1 - \int_0^{\pi} \cos(2(\theta - \theta_{p,\text{exp}})) f_{\text{exp}}(\theta) d\theta \quad (1)$$

where $f_{\text{exp}}(\theta)$ is the experimentally determined fiber distribution function, normalized such that $\int_0^{\pi} f_{\text{exp}}(\theta) d\theta = 1$. Note that we consider fiber orientation angles, θ , including $\theta_{p,\text{exp}}$, to lie in the interval $[0, \pi)$. Further, note that var_{exp} as defined in (1) equals the 2D version of the dispersion parameter defined by Gasser et al. (2006) and derived by Grytz and Meschke (2010) multiplied by $\pi/2$.

The goal was to robustly fit the experimental data using a function $f(\theta; p_1, \dots, p_n)$ of n parameters p_i such that at each experimental point, a set of parameters p_i exists.

2.1 Choice of a modeling function and cost minimization approach

The function f should be as simple as possible, i.e. have as few parameters as possible, while still robustly fitting the data for the entire tissue, and be physically meaningful. Based on previous work with ideal fiber characteristics, the π -periodic von Mises distribution was used for its simplicity (Nguyen and Boyce; Gasser et al. 2006; Pandolfi and Holzapfel 2008; Girard et al. 2009a,b,c; Raghupathy and Barocas 2009; Cortes et al. 2010; Grytz and Meschke 2010;

Grytz et al. 2010) as it can describe fiber organization with only two parameters (Fisher 1993)

$$f(\theta; k, \theta_p) = \frac{1}{\pi I_0(k)} \exp(k \cos(2(\theta - \theta_p))) \quad (2)$$

where I_0 is the modified Bessel function of the first kind of order zero and k is the so-called fiber concentration factor, characterizing the spread of the fiber distribution around the preferred orientation θ_p .

Initial examination showed the existence of an additional constant component in the fiber distribution data, corresponding to an isotropic subpopulation of fibers as observed in other tissues (Ferdman and Yannas 1993; Abahussin et al. 2009). The function (2) was therefore modified, and after normalization over the interval $[0, \pi)$ took the form:

$$f(\theta; \beta, k, \theta_p) = \frac{1 - \beta}{\pi} + \frac{\beta}{\pi I_0(k)} \exp(k \cos(2(\theta - \theta_p))) \quad (3)$$

where β , a parameter bounded by 0 and 1, weights the proportion of isotropic and anisotropic contributions. For $\beta = 0$, the fibers are isotropically dispersed regardless of the value of k , while k is a measure of anisotropy, but only with respect to the von Mises subpopulation of fibers. In general, therefore, changes in the values of either β or k will result in a change in the semi-circular variance computed from the function f , i.e. a change in the measure of fiber anisotropy. We denote the semi-circular variance computed from the analytic expression for f (i.e. with f replacing f_{exp} in equation (1)) as $\text{var}_{\text{model}}$.

The fitting of eq. (3) to the experimental data is an optimization problem. The following cost function was defined:

$$\text{cost}(\beta, k, \theta_p) = \frac{1}{n} \sqrt{\sum_{i=1}^n \left(\frac{f(\theta_i; \beta, k, \theta_p) - f_{\text{exp}}(\theta_i)}{(f(\theta_i; \beta, k, \theta_p) + f_{\text{exp}}(\theta_i))/2} \right)^2} \quad (4)$$

where f_{exp} , the experimentally determined fiber distribution, is assumed to be known at n angles θ_i . Thus, at each experimental point, fitting the model function f to the experimental values involves finding the set of parameters (β, k, θ_p) for which the cost is minimum, which was solved with the differential evolution genetic optimization algorithm (Price et al. 2005).

2.2 Experimental methods

For initial tests, we used experimental data obtained from SALS on rat sclera (Girard et al. 2010). Briefly, one patch of scleral tissue (overlapping anterior, equatorial and posterior regions) from a normal rat eye was dissected and cleared in a glycerol solution. The patch was laid flat between two microscope slides, mounted in a custom holder, and scanned

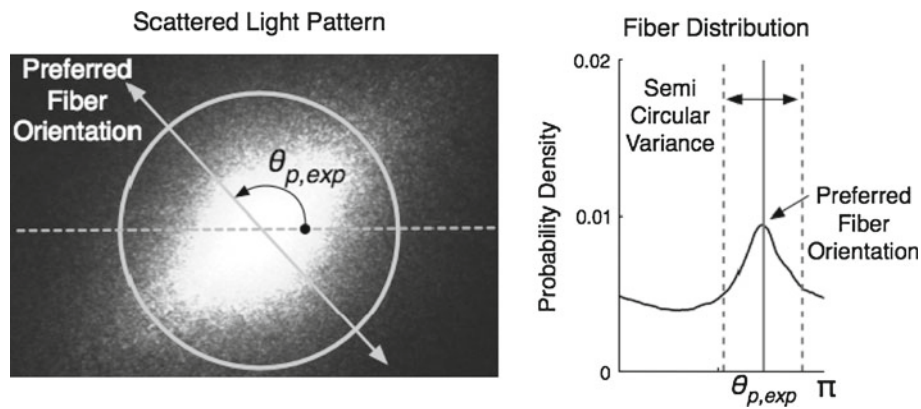


Fig. 1 Typical small-angle light scattering data pattern at a single point (*left*). The light intensity on a superimposed circle centered with respect to the diffraction pattern, nominally proportional to collagen fiber density, gives the experimental fiber probability distribution, which

is shown at right as a function of angle θ . The data on opposite sides of the *circle*, i.e. at θ and $\theta + \pi$, are averaged to give a single value at each θ in the interval $[0, \pi)$. $\theta_{p,exp}$ is the experimentally determined preferred fiber orientation

at multiple locations (100 μm spacings) with a 5-mW HeNe laser beam (diameter: 0.5 mm; wavelength: 632.8 nm). The laser light was scattered by scleral fibers (mainly collagen) and projected onto a diffuser screen. Snapshots of scattered light intensity were recorded by a monochrome CCD camera (1024 \times 768, 16-bit pixels) and analyzed digitally using custom Matlab functions in order to extract fiber distributions at each scanned location. A typical scattered light intensity pattern is shown in Fig. 1, with its corresponding fiber distribution. We have also carried out fitting on SALS data from other tissues, and on data gathered using nonlinear optical microscopy (see Sect. 3.4).

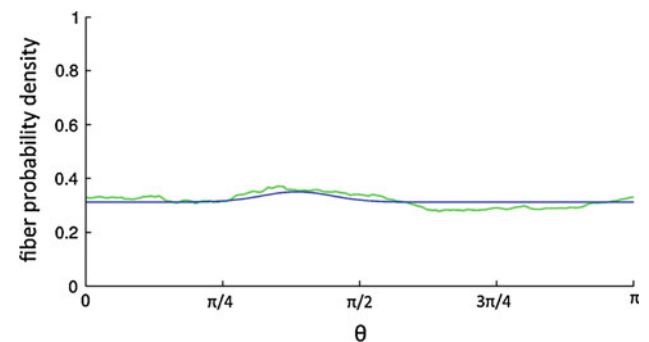


Fig. 2 Comparison of the experimentally measured fiber distribution (*green*) and the fitted distribution (*blue*). The value of var_{exp} was 0.95, which corresponds to nearly complete planar isotropy. Accordingly, a small β was obtained ($\beta = 0.01$), but k was unexpectedly high ($k = 5.5$)

2.3 Fitting approaches

Within the above framework, we considered three possible fitting approaches.

2.3.1 An unconstrained (three-parameter) approach

The simplest approach is simply to fit equation (3) to the data using the cost function in equation (4), without constraining any of the parameters (β, k, θ_p).

2.3.2 A constrained (two-parameter) approach

Unfortunately, preliminary tests showed that the unconstrained approach gave poor results, particularly in regions where there was a high degree of isotropy in the data (large var_{exp}) and noise was present. Similar problems typically did not occur at points with small var_{exp} , where there was proportionally larger peaks (i.e. lower signal-to-noise ratio). For example, Fig. 2 shows experimental data and fitted curves for one such location. Since the experimentally measured fiber

distribution was almost constant, the fitting procedure set the exponential part of the model to be almost zero (β very small). However, to fit the peak, a very large k was needed to compensate for the small β , even though the peak was almost non-existent and due mostly to experimental noise. Thus, by minimizing the cost function for the distribution in equation (3), the algorithm produced a non-physical outcome due to only a modest amount of experimental noise. In such regions, the algorithm produced values of either β or k that were very large and varied sharply from between adjacent regions. Large values of k and rapid parameter variations are expected to be undesirable since they could lead to poor conditioning in numerical simulations based on extracted parameters.

We also observed non-uniqueness of (β, k) pairs obtained from fitting. For example, in Fig. 3, both fitted distributions were obtained from the same experimental data; however, the blue fitted curve had significantly different (β, k) values compared to the magenta fitted curve, even though the cost of the two fits was the same and was small (0.7%). Since a

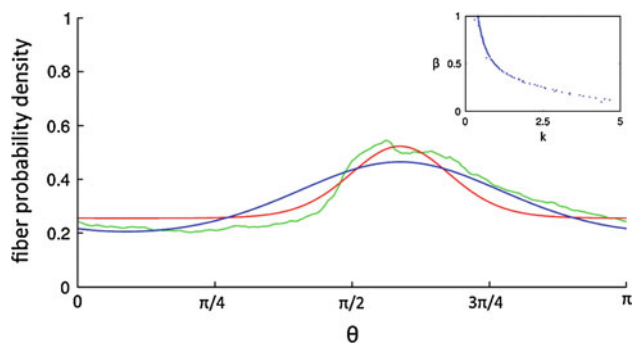


Fig. 3 Comparison of the experimentally measured fiber distribution (green; $\text{var}_{\text{exp}} = 0.92$) and the fitted distributions (blue and red). The blue and red fits have different parameter values ($\beta = 0.2$; $k = 3.1$) and ($\beta = 0.8$; $k = 0.5$), for reasons described in the text. The inset shows the entire family of non-unique (β, k) fitting pairs for the experimental data produced by the unconstrained fitting algorithm

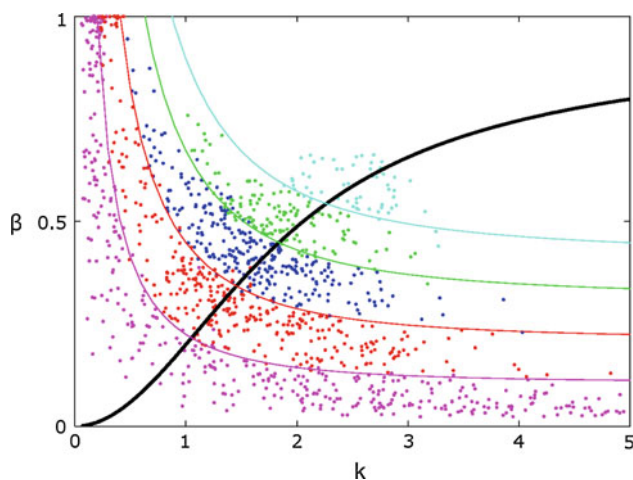


Fig. 4 Values of β and k obtained from fitting an experimental data set. Each point represents the results of the fitting at a single location within the tissue, colored according to the variance in the data at that point: magenta: $\text{var}_{\text{exp}} > 0.9$; red: $0.8 < \text{var}_{\text{exp}} < 0.9$; blue: $0.7 < \text{var}_{\text{exp}} < 0.8$; green: $0.6 < \text{var}_{\text{exp}} < 0.7$; cyan $\text{var}_{\text{exp}} < 0.6$. Note that regions with larger anisotropy, corresponding to smaller var_{exp} (cyan and green), lie in a narrower range of (β, k) values. Colored lines represent the theoretical (β, k) pairs (see equation (9)) for $\text{var}_{\text{exp}} = 0.9$ (magenta), $\text{var}_{\text{exp}} = 0.8$ (red), $\text{var}_{\text{exp}} = 0.7$ (green) and $\text{var}_{\text{exp}} = 0.6$ (cyan). The black line represents the constraint shown in eq. (5)

given non-constant modified von Mises distribution can be described by only one (β, k) pair, the two pairs that were obtained do not correspond to the same model distribution. This undesirable non-uniqueness comes from the multiple ways experimental data can be fit by the genetic optimization algorithm when the fitting problem is poorly posed, which in turn arises due to the use of random seeds in the optimization algorithm. In fact, by running the fitting algorithm multiple times, we were able to find a whole family of (β, k) couples fitting the experimental data at a reasonable cost of $\leq 1\%$ (Fig. 3, inset).

The above examples show that it would be beneficial if the fitting approach was further constrained, especially in the presence of noise. Further, preliminary tests showed that $\theta_p \approx \theta_{p,\text{exp}}$, implying that the algorithm was accurately fitting the preferred fiber orientation. Therefore, we focused attention on constraining β and k . There are some general principles that such a constraint must satisfy. Since in most cases, changes in either β or k result in a change in the semi-circular variance $\text{var}_{\text{model}}$ (i.e. a change in anisotropy), we decided to define both parameters as explicit measures of anisotropy in order to limit any aforementioned incoherent behavior. Accordingly, we required $\beta = 1$ when $k = 0$ (planar isotropy or $\text{var}_{\text{model}} = 0$). Further, when $\beta = 1$ (transverse anisotropy or $\text{var}_{\text{model}} = 1$), we required k to be infinity, corresponding to a delta function for $f(\theta; \beta, k, \theta_p)$. Finally, we observed empirically that at locations with large anisotropy (and hence relatively better signal-to-noise ratios), the range of (β, k) fitting pairs obtained from the genetic optimization algorithm was narrow (Fig. 4), and it is clear that any constraint should pass through this empirically determined range.

Although there are infinitely many constraints between β and k that satisfy the above principles, we also wanted an expression that was computationally efficient. After testing a number of possibilities, we found that the following relationship gave very satisfactory results

$$\beta = \left(\frac{I_1(k)}{I_0(k)} \right)^n \tag{5}$$

where I_1 is the modified Bessel function of the first kind of order one and n is a tissue-dependent parameter. For all fitting of SALS data on rat sclera, we used $n = 2$. Using Eq. (5), Eq. (3) can be rewritten as:

$$f_{\text{constrained}}(\theta; k, \theta_p) = \frac{1}{\pi I_0(k)^2} \left(I_0(k)^2 - I_1(k)^2 + \frac{I_1(k)^2}{\pi I_0(k)} \exp(k \cos(2(\theta - \theta_p))) \right) \tag{6}$$

and this function was used in Eq. (4) in place of f .

2.3.3 A direct two-parameter approach

Motivated by the observed relationship between β and k for a given level of variance in a data set, we developed a third approach that involved an analytic relationship between β, k and var_{exp} . The semi-circular variance of a modified von

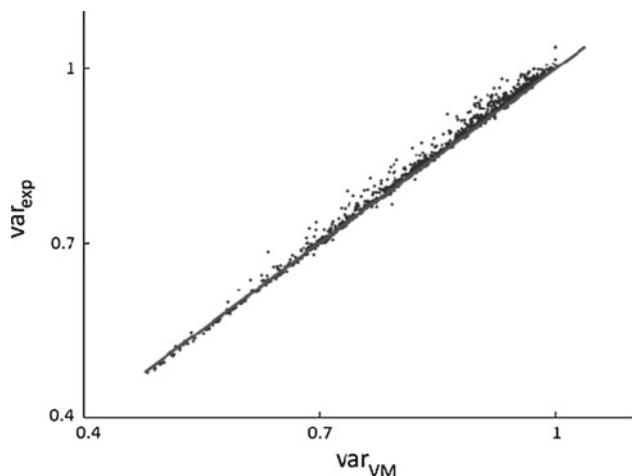


Fig. 5 A plot of the experimentally determined variance, var_{exp} , versus the theoretically expected value, $\text{var}_{\text{VM}} = 1 - \beta \frac{I_1(k)}{I_0(k)}$. Here, (β, k) couples were obtained from the constrained two-parameter model. The line is the line of identity. See text for full details

Mises distribution characterized by parameters (β, k, θ_p) is:

$$\begin{aligned} \text{var}_{\text{VM}} &= 1 - \int_0^\pi \cos(\theta - \theta_p) \\ &\times \left(\frac{1 - \beta}{\pi} + \frac{\beta}{\pi I_0(k)} \exp(k \cos(2(\theta - \theta_p))) \right) d\theta \\ &= 1 - \beta \frac{I_1(k)}{I_0(k)} \end{aligned} \tag{7}$$

where I_1 is the modified Bessel function of the first kind of order one. A suitable fitting should lead to a modeled variance which is comparable to the experimental one. Hence, we assume that we can set var_{exp} equal to var_{VM} giving:

$$\text{var}_{\text{exp}} = 1 - \beta \frac{I_1(k)}{I_0(k)} \tag{8}$$

Rearrangement gives an expression for β in terms of the other fitting parameter k and the experimentally determined var_{exp} :

$$\beta = (1 - \text{var}_{\text{exp}}) \frac{I_0(k)}{I_1(k)} \tag{9}$$

One way to check the validity of the assumption underlying this approach is to plot var_{exp} against var_{VM} as defined by Eq. (7). Figure 5 shows this comparison, and we can see that the assumption that $\text{var}_{\text{exp}} = \text{var}_{\text{VM}}$ is indeed a good one.

Equations (5) and (9) are a system of two equations for β and k , which can be solved

$$\beta = (1 - \text{var}_{\text{exp}})^{2/3} \tag{10}$$

$$\left(\frac{I_1(k)}{I_0(k)} \right)^2 = \beta \tag{11}$$

Thus, a third approach is to calculate β from the experimental value of var_{exp} and then use equation (11) to find k . In this approach, the fiber orientation θ_p was forced to be equal to the experimentally determined angle $\theta_{p,\text{exp}}$. Note that in this approach, there is no minimization of a cost function.

3 Results

In order to get a global overview of the quality of the fit, it is useful to plot maps of the experimental data $(1 - \text{var}_{\text{exp}}, \theta_{p,\text{exp}})$ and of the parameters (β, k, θ_p) at each measurement location (Fig. 6). The quantity $1 - \text{var}_{\text{exp}}$ was used because it allows comparison with the model characteristic k ; more specifically $1 - \text{var}_{\text{exp}}$, decreases when isotropy increases, as should k for non-zero β . We also examined maps of the cost, a local measure of the relative error of the fit.

3.1 The unconstrained (3-parameter) fitting approach

The results obtained with the three-parameter model, i.e. with (β, k, θ_p) unconstrained, show that the fitted values of the fiber orientations, θ_p , obtained by the model were very close to the experimental values (Fig. 6); however, the values of β and k were disappointing as they were found to be randomly discontinuous across the tissue sample (for reasons discussed in Sect. 2.3.2), suggesting that they do not represent physically meaningful values. For example, in the bottom left corner of the patch, the cost was very low, whereas high values of k (non-physically meaningful) were obtained in this isotropic zone. This situation and others not presented here showed that the cost can be a misleading indicator of fit quality, and should be used cautiously, in combination with other criteria such as maps of the values of β and k .

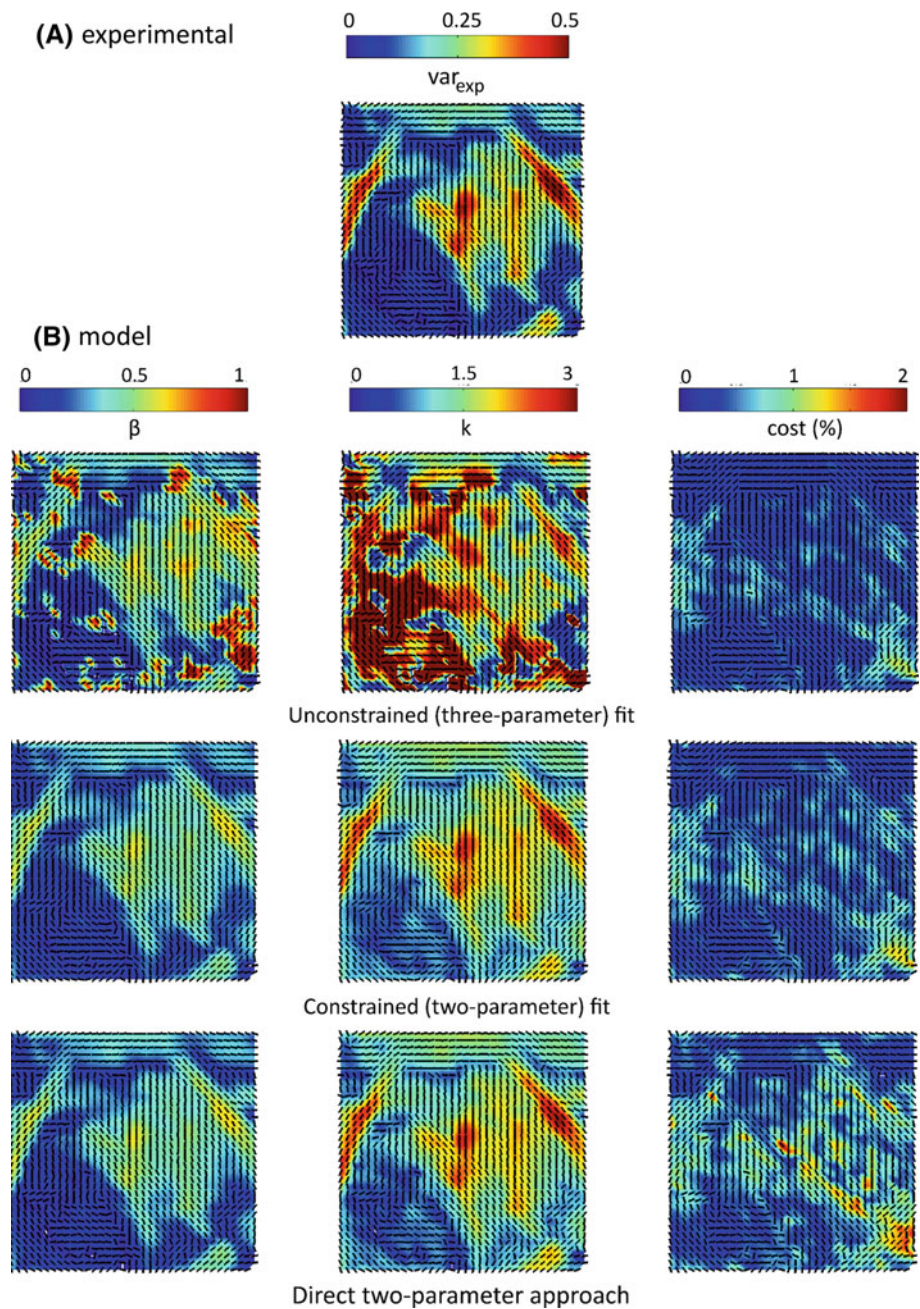
3.2 The constrained (2-parameter) fitting approach

With this approach, the fiber orientations were well fit and the cost remained reasonably low. The cost was higher in some regions than for the 3-parameter approach, but this was not surprising since the fit was more constrained. The quantities β and k reflected the anisotropic properties of the tissue very well. It is worth noting that the maps of β, k and var_{exp} are not expected to be identical but rather are different ways of measuring anisotropy. The key points are that the fitting smoothed the experimental noise, and that the global regions of anisotropy and isotropy were well modeled.

3.3 The direct (2-parameter) approach

In this approach, the “fitted” preferred (modal) fiber orientations were of course identical to the experimental ones. The

Fig. 6 **a** Map of the experimentally measured fiber distribution characteristics over a square tissue region. The preferred fiber orientations, $\theta_{p,exp}$, are represented by *black lines* and $1 - \text{var}_{exp}$ (a measure of anisotropy) by the *color scale*. **b** Results of the three different fitting approaches as applied to the experimental data shown in **a**. The preferred fiber orientations are represented by *black lines* and the values of the quantity of interest (β , k or cost) by the *color scales*. See text for explanation of the different fitting approaches



values of β and k appeared to be very close to the values obtained with the constrained (2-parameter) model, which is reassuring. However, the slight differences between the 2-parameter model and the direct calculation were enough to lead to a significant increase in the cost values at some locations. Figure 7 shows a typical situation occurring at such a location. Because of noise near the peak of the experimental data, the experimental characteristics were inaccurately fit. In particular, a shift in $\theta_{p,exp}$ was observed, which directly impacted the fit (and its quality) since θ_p was simply taken equal to $\theta_{p,exp}$. Because of this effect, the direct approach

was felt to be inferior to the constrained (2-parameter) fitting approach.

3.4 Other tissue types and imaging approaches

The fitting results presented to this point have all used SALS data obtained from rat sclera. However, it is of interest to consider fitting data from other tissues and also data gathered by modalities other than SALS. We therefore fit the fiber distribution data of Timmins et al. (2010), gathered using nonlinear optical microscopy that visualized collagen and elastin fibers

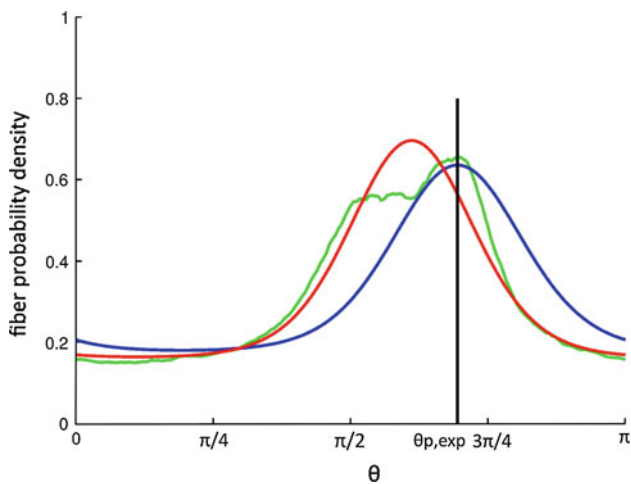


Fig. 7 Plot of fiber probability density vs fiber orientation angle at a single location. *Green*: experimental data; *blue*: the results of the direct approach for fitting the data; *red*: the results of the constrained (2-parameter) fitting approach. The experimental quantities var_{exp} and $\theta_{p,\text{exp}}$ do not smooth the noise at the peak, and hence the direct approach is influenced by this noise. However, the fit obtained by the constrained (2-parameter) model smoothes the noise and gives a better global fit to the experimental data

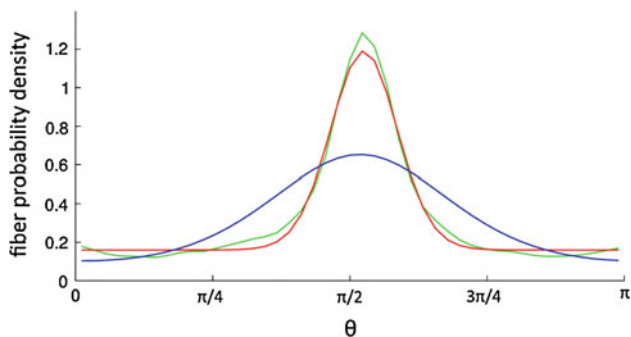


Fig. 8 Experimental fiber distribution (*green*) for one location of the inner medial region of a bovine common artery obtained using non-linear optical microscopy (Timmins et al. 2010). The curve in *red* is the best fit using our constrained (2-parameter) approach with $n = 8$, while the curve in *blue* is the one from the “standard” semi-circular von-Mises defined in Eq. (2). This graph demonstrates that our constrained (2-parameter) approach can accurately describe 2D fiber organization in a tissue where the “standard” semi-circular von-Mises distribution does not yield a good fit

in the inner medial region of bovine common carotid arteries. We fitted these data with both our constrained (2-parameter) approach (using an exponent $n = 8$ in Eq. (5)) and the “standard” semi-circular von-Mises distribution, obtaining a good fit only with the constrained (2-parameter) approach (Fig. 8).

We have also carried out analyses using other tissues (cornea, lamina cribrosa, cortical bone, cartilage) from multiple species, with similar results. However, it is important to note that the optimal value of the exponent n in the constraint Eq. (5) appears to be tissue dependent. For example,

we found that best results were obtained with $n = 2$ for rat sclera, $n = 1$ for bovine sclera and $n = 8$ with bovine artery data. The determination of a suitable value for n is empirical, e.g. based on analysis of data such as shown in Fig. 4.

4 Discussion and conclusions

We have presented a method for fitting experimental measurements of fiber distribution in tissue samples, necessary for e.g. finite element modeling of tissue biomechanics. We chose the two-parameter π -periodic circular von Mises distribution for the fitting, based on its physical meaning and simplicity. However, it was necessary to modify this distribution to take into account an isotropic fiber subpopulation present in the experimental data. Unfortunately, the additional degree of freedom inherent in this modified distribution led to problems of uniqueness and non-physical fitting, which were overcome by adding a constraint to the fitting process.

The constrained version of the fiber distribution function (Eq. (6)) was chosen partly based on empirical observations (Fig. 5). However, it was checked on a number of samples (e.g. bone, lamina cribrosa, cornea, arteries) and gave the best results from among the many candidate constraints considered. Nonetheless, we suggest that it would be prudent to check the suitability of this constraint prior to use of this approach in other tissue types. This could be accomplished by carrying out an unconstrained (3-parameter) fit, and plotting the parameter maps (Fig. 6) and (β, k) scattering diagrams (Fig. 4). We suggest that constraints of the form of (equation 5) should be suitable for most situations. Indeed, decreasing or increasing n will move the constraint curve up or down in Fig. 4 to pass through the range of (β, k) pairs determined from the 3-parameter fit. For example, the use of $n = 1$ with bovine scleral data, $n = 2$ for rat sclera data and $n = 8$ with bovine artery data provided the best performance overall. These different optimal values of n could possibly reflect differences in the fibrous structure of the tissue, a hypothesis that warrants further investigation.

The direct approach may seem very attractive, since it provides expressions for the fitting parameters without a minimization process, making it quicker than the constrained (2-parameter) approach (typically about tenfold faster). However, it must be kept in mind that the fitting process smoothed noise in the experimental data and gave a better overall result. Because the overall computational burden associated with the fitting was not particularly large, we recommend the constrained (2-parameter) approach.

Acknowledgments We thank Dr Lucas Timmins for providing the raw data on fiber distribution in the arterial wall.

References

- Abahussin M, Hayes S et al (2009) 3D collagen orientation study of the human cornea using X-ray diffraction and femtosecond laser technology. *Invest Ophthalmol Vis Sci* 50(11):5159–5164
- Aghamohammadzadeh H, Newton RH et al (2004) X-ray scattering used to map the preferred collagen orientation in the human cornea and limbus. *Structure* 12(2):249–256
- Bowes LE, Jimenez MC et al (1999) Collagen fiber orientation as quantified by small angle light scattering in wounds treated with transforming growth factor-beta2 and its neutralizing antibody. *Wound Repair Regen* 7(3):179–186
- Chien JCW, Chang EP (1972) Small-angle light scattering of reconstituted collagen. *Macromolecules* 5(5):610–617
- Cortes DH, Lake SP et al (2010) Characterizing the mechanical contribution of fiber angular distribution in connective tissue: comparison of two modeling approaches. *Biomech Model Mechanobiol* 9(5):651–658
- Ferdman AG, Yannas IV (1993) Scattering of light from histologic sections: a new method for the analysis of connective tissue. *J Invest Dermatol* 100(5):710–716
- Fisher NI (1993) *Statistical analysis of circular data*. Cambridge University Press, Cambridge
- Fung YC (1993) *Biomechanics mechanical properties of living tissues*. Springer, New York
- Gasser TC, Ogden RW et al (2006) Hyperelastic modelling of arterial layers with distributed collagen fibre orientations. *J R Soc Interface* 3:15–35
- Girard MJ, Dahlmann A et al (2010) Quantitative mapping of scleral fiber orientation in normal rat eyes. *Invest Ophthalmol Vis Sci* 51(5):2128
- Girard MJ, Downs JC et al (2009) Peripapillary and posterior scleral mechanics-part II: experimental and inverse finite element characterization. *J Biomech Eng* 131(5):051012
- Girard MJ, Downs JC et al (2009) Peripapillary and posterior scleral mechanics-part I: development of an anisotropic hyperelastic constitutive model. *J Biomech Eng* 131(5):051011
- Girard MJ, Suh JK et al (2009) Scleral biomechanics in the aging monkey eye. *Invest Ophthalmol Vis Sci* 50(11):5226–5237
- Grytz R, Meschke G (2010) A computational remodeling approach to predict the physiological architecture of the collagen fibril network in corneo-scleral shells. *Biomech Model Mechanobiol* 9(2):225–235
- Grytz R, Meschke G et al (2010) The collagen fibril architecture in the lamina cribrosa and peripapillary sclera predicted by a computational remodeling approach. *Biomech Model Mechanobiol*
- Hayes S, Boote C et al (2007) A study of corneal thickness, shape and collagen organisation in keratoconus using videokeratography and X-ray scattering techniques. *Exp Eye Res* 84(3):423–434
- Joyce EM, Liao J et al (2009) Functional collagen fiber architecture of the pulmonary heart valve cusp. *Ann Thorac Surg* 87(4):1240–1249
- McCally RL, Farrell RA (1982) Structural implications of small-angle light scattering from cornea. *Exp Eye Res* 34(1):99–113
- Meek KM, Boote C (2009) The use of X-ray scattering techniques to quantify the orientation and distribution of collagen in the corneal stroma. *Prog Retin Eye Res* 28(5):369–392
- Nguyen TD, Boyce BL (2011) An inverse finite element method for determining the anisotropic properties of the cornea. *Biomech Model Mechanobiol* 10(3):323–337
- Pandolfi A, Holzapfel GA (2008) Three-dimensional modeling and computational analysis of the human cornea considering distributed collagen fibril orientations. *J Biomech Eng* 130(6):061006
- Pierce DM, Trobin W et al (2010) DT-MRI based computation of collagen fiber deformation in human articular cartilage: a feasibility study. *Ann Biomed Eng* 38(7):2447–2463
- Price KV, Storn RM et al (2005) *Differential evolution. A practical approach to global optimization*. Springer, Berlin
- Raghupathy R, Barocas VH (2009) closed-form structural model of planar fibrous tissue mechanics”. *J Biomech* 42(10):1424–1428
- Roberts MD, Grau V et al (2008) Remodeling of the Connective Tissue Microarchitecture of the Lamina Cribrosa Occurs Early in Experimental Glaucoma in the Monkey Eye. *Invest Ophthalmol Vis Sci* 50(2):681–690
- Sacks MS, Smith DB et al (1997) A small angle light scattering device for planar connective tissue microstructural analysis. *Ann Biomed Eng* 25(4):678–689
- Timmins LH, Wu Q et al (2010) Structural inhomogeneity and fiber orientation in the inner arterial media. *Am J Physiol Heart Circ Physiol* 298(5):H1537–H1545